A multi-modal adaptive tuned mass damper based on shape memory alloys

Marta Berardengo[1], Giovanni EP Della Porta[2], Stefano Manzoni[2] and Marcello Vanali[1]

Abstract

This article deals with the design of an innovative adaptive multi-modal tuned mass damper able to change its eigenfrequencies to recover shifts of the natural frequencies of the primary system which needs to be damped. This is accomplished using systems of shape memory alloy wires connected to a number of masses equal to the number of modes to be damped. This article presents the analytical model used to describe the behaviour of the adaptive tuned mass damper, showing which parameters can affect the performances of the device. The layout proposed for the tuned mass damper proves to be able to act on a wide frequency range and to work adaptively on at least two eigenfrequencies at the same time with a given level of independence. The last goal is accomplished, thanks to the special features of the shape memory alloys, by heating (or cooling) each wire of the device independently and allowing the exploitation of two different effects: the change of the axial load in the wires and the change of the geometry of the device. The reliability of both the design approach and the model of the new device is proved by means of an experimental campaign performed considering a random disturbance.

Keywords

Tuned mass damper, multi-modal tuned mass damper, adaptation, shape memory alloys, vibration, damping, vibration control

Introduction

On account of their advantageous features, the use of smart materials for vibration reduction has proved to be very promising. Indeed, piezoelectric materials (e.g. Berardengo et al., 2015b, 2016, 2017a, 2017b; Heuss et al., 2016; Høgsberg and Krenk, 2015), shape memory alloys (SMAs; e.g. Casciati et al., 2014; Dieng et al., 2013; dos Santos and Nunes, 2018; Mavroidis, 2002; Ozbulut et al., 2007; Piccirillo et al., 2016; Saggin et al., 2017; Senthilkumar and Umapathy, 2013; Torra et al., 2014), magnetic memory alloys (e.g. Majewska et al., 2007), and magnetorheological materials (e.g. Caterino et al., 2011; Weber and Maślanka, 2012) have been fruitfully employed in damping and actuation applications.

These materials were shown to be effective for the design of semi-active and active tuned mass dampers (TMDs). In general, TMDs reduce vibrations very effectively, but they have two main drawbacks: (1) their performances decrease significantly when mistuning occurs and (2) they usually act on a single mode. With regard to the first point, smart materials can give significant contributions because their properties are particularly suitable for the design of adaptive TMDs (e.g. Heuss et al., 2016). Adaptive TMDs able to adapt their own eigenfrequencies can follow the changes of one eigenfrequency of the primary system to be damped, allowing the adaptive TMD to be always tuned and to achieve an optimal damping action (e.g. Weber, 2013). Changes in the dynamical features of the primary system are a critical issue since they often occur because of a number of possible reasons (e.g. thermal shifts).

Among the various smart materials, this article focuses on the use of SMAs. Indeed, SMAs have been successfully employed to damp vibrations in light structures, and especially to design and construct adaptive TMDs capable of changing their eigenfrequency, on

[1]Department of Engineering and Architecture, Università degli Studi di Parma, Parma, Italy
[2]Department of Mechanical Engineering, Politecnico di Milano, Milan, Italy

Corresponding author:
Stefano Manzoni, Department of Mechanical Engineering, Politecnico di Milano, Via La Masa 34, 20156 Milan, Italy.
Email: stefano.manzoni@polimi.it

account of the unique physical properties of such materials.

Furthermore, they are cheaper than other materials and can be manufactured in shapes (e.g. wires) which guarantee low weights; this is a key characteristic because adaptive devices can be designed and built in a manner that avoids high load effects in light structures.

Several works on adaptive devices based on SMAs have been proposed in the literature to demonstrate the possibility of applying SMA-based devices in real engineering applications. As examples, Mani and Senthilkumar developed an application where an absorber made from SMA springs damps the vibration of a centrifugal pump with varying excitation frequency (Mani and Senthilkumar, 2013), while Zuo and Li demonstrated that SMA dampers are suitable for mitigating cable vibrations (Zuo and Li, 2011). The various works proposed by the scientific community on adaptive TMDs based on SMAs differ in the principle used to adapt the TMD eigenfrequency and in the control strategy that is applied. For example, Rustighi et al. showed the effectiveness of cantilever beams made from SMA material to build reliable adaptive TMDs (Rustighi et al., 2005a). Changes in the eigenfrequency of the adaptive TMD occur when the SMA material temperature is changed, which in turn causes a change in its Young's modulus. Different strategies for controlling this type of adaptive TMD are presented in Rustighi et al. (2005b). Williams et al. developed an adaptive TMD based on a series of SMA-based cantilever beams in Williams et al. (2002), relying on the same physical principle presented in Rustighi et al. (2005a). Then, Williams et al. discussed a non-linear control approach for the same device in Williams et al. (2005). A different approach is discussed by Savi et al., who studied the behaviour of an SMA spring to be used for vibration control (Savi et al., 2010), evidencing its capability to change stiffness and damping properties by changing temperature and exploiting the pseudoelastic effect (see the next section). A similar device was studied experimentally by Aguiar et al. (2012). Tiseo et al., instead, showed experimentally that an adaptive TMD can be built with an SMA wire with constrained ends and with a mass located at its centre. Indeed, the eigenfrequency of the system can be changed by changing the temperature of the wire (Tiseo et al., 2010). Despite the effectiveness of the presented design and working principle, no models of the structure, control criteria and quantification of the adaptation performances were addressed in this work.

Recently, Berardengo et al. (2014, 2015a) proposed a new SMA-based adaptive TMD able to change its eigenfrequency by more than 100% of its initial value, by coupling elastic elements to SMA wires and a central mass. Furthermore, this adaptive TMD layout showed to have two further advantages when compared to the other SMA-based adaptive TMDs: (1) it works properly with any kind of SMA material, therefore without requiring high-performance SMAs (i.e. SMAs with special features such as high change of Young's modulus with temperature); (2) devices that change the damping level of the adaptive TMD can be easily added. This was accomplished in Berardengo et al. (2015a) using an eddy current damper, but other systems/principles could be used (e.g. magnetic devices (Dai et al., 2014) or mechanical devices).

Albeit the effectiveness of SMAs in the development of adaptive TMDs is proved by the referenced works, the other main drawback of these adaptive TMDs (i.e. they usually act on a single mode, as above-mentioned) is still an open issue. Indeed, there is a lack of works in the literature proposing adaptive TMDs based on smart materials able to work at the same time on more than one mode of the primary system independently. In this scenario, the goal of this article is to investigate the possibility of designing SMA-based adaptive TMDs that can change more than one eigenfrequency in specific frequency ranges independently and at the same time (multi-modal adaptive TMDs). This would give an adaptive TMD able to recover any possible change in the primary system eigenfrequencies, thus assuring satisfactory damping of the vibrations of the primary system. The working principle and the design approach are the same as those described in Berardengo et al. (2015a), because the device proposed there guarantees high layout flexibility and an extended frequency range when compared to the other SMA-based adaptive TMDs.

This article is structured as follows. The next two sections recall the SMA features and the SMA-based adaptive TMD presented in Berardengo et al. (2015a), respectively, for understanding the newly proposed multi-modal adaptive TMD. Then, this multi-modal adaptive TMD is presented, discussing how SMA properties are used to design it and developing its analytical model. The last two sections of this article discuss the adaptive TMD performances by means of numerical simulations and validate the results through an experimental campaign, respectively.

SMAs

This section recalls the main properties of SMAs (Lagoudas, 2008) useful for understanding the working principle of the proposed adaptive device. SMAs are characterised by transformations over three different solid phases, which occur when the material undergoes a change of either temperature or applied stress. The solid phase transition leads to changed mechanical properties (e.g. Young's modulus) and can cause a change in the SMA shape. The three phases involved in these transformations are detwinned martensite (DM), twinned martensite (TM) and austenite (AU).

Table 1. Experimentally identified data for the SMA material used in this work.

A_s	A_f	M_s	M_f	C_A	C_M	H^{cur}	$E_{w,\,DM}$	$E_{w,\,AU}$	α
68.6 °C	78.9 °C	55.2 °C	42.7 °C	9.90 MPa/°C	6.83 MPa/°C	4.39%	32.1 GPa	39.5 GPa	10^{-6} °C^{-1}

SMA: shape memory alloy.

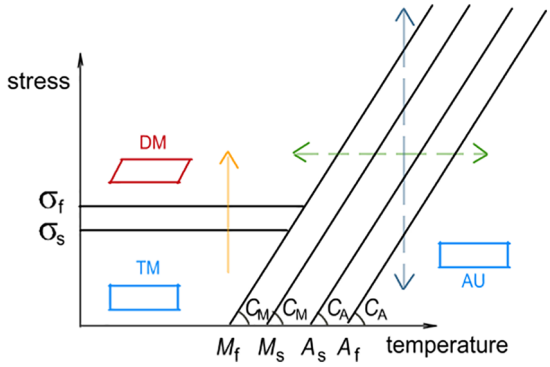

Figure 1. Temperature–stress diagram of SMA materials.

Figure 1 shows the phase diagram of SMA, where σ_s is the stress value at which the transformation from TM to DM starts at environmental temperature, while σ_f is the stress value at which the transformation is completed. Furthermore, A_s is the temperature value at which the transformation from TM to AU starts at null stress, A_f is the value at which the transformation is completed, M_s is the temperature value at which the transformation from AU to TM starts at null stress and M_f is the value at which the transformation is completed. C_A and C_M are the angular coefficients of the transformation lines. Table 1 gathers the values of the parameters shown in Figure 1 for the SMA wires used in this work (identified experimentally), which are made of Nitinol (nickel and titanium). In Table 1, H^{cur} is the strain due to the change of shape during the change of phase between TM and DM (see the vertical solid arrow in Figure 1), named the current maximum transformation strain; α is the thermal expansion coefficient. Finally, $E_{w,\,DM}$ and $E_{w,\,AU}$ are Young's moduli of the DM and AU phases, respectively.

Figure 1 shows that the shape of the SMA can be changed when either transformations from TM to DM occur or the SMA changes phase from DM to AU and vice versa. The shape in the TM and AU phases is almost the same (i.e. unstrained). Therefore, a shape change can be obtained by applying a stress value higher than σ_s (transformation from TM to DM, see the vertical solid arrow in Figure 1) and the original shape can be recovered by increasing the temperature (transformation from DM to AU). When the SMA is in the AU phase, the shape can be changed by exploiting the AU-DM transformation (and vice versa) and thus by changing the temperature (temperature-induced phase transformation, see the horizontal dashed double arrow in Figure 1) and/or the applied stress (pseudoelastic effect, see the vertical dashed double arrow in Figure 1).

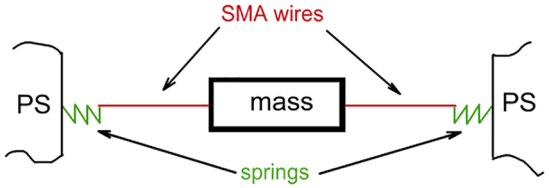

Figure 2. Layout of the SMA-based original adaptive TMD. Primary system abbreviated as PS in the figure.

The strain of the SMA wires ε_w can be expressed by the following general relation according to Lagoudas (2008)

$$\varepsilon_w = \varepsilon_w^e + \varepsilon_w^t + \varepsilon_w^{th} \quad (1)$$

where ε_w^{th} is the strain component due to thermal expansion, ε_w^e is the elastic strain component and ε_w^t is the strain component due to the thermoelastic martensitic transformation (i.e. the strain caused by the change of shape from TM to DM; refer to Figure 1).

Adaptive TMD

As mentioned, the multi-modal adaptive TMD presented in this work takes advantage of the adaptive TMD proposed by Berardengo et al. (2015a). Consequently, it is worthwhile to recall its working principle briefly.

The adaptive TMD presented in Berardengo et al. (2015a) relies on the use of two (or more) SMA wires, a central mass and some elastic elements (see Figure 2). The elastic elements link this adaptive TMD to the primary system to be damped and make it possible to apply a pre-stress (and thus a pre-strain) to the wires. The value of this pre-stress is set above σ_f (see Figure 1) in order to have the SMA wires in the DM condition. Therefore, a further change in the shape (i.e. mainly the length) of the wires can be achieved by means of a temperature change, relying on the transformation between DM and AU. Since the wires are constrained to the primary system through elastic elements, this change of shape also changes the axial tensile load F that the wires

are subject to, which in turn changes the first eigenfrequency of the adaptive TMD (Acar and Yilmaz, 2013; Meirovitch, 2001; Rainieri and Fabbrocino, 2015). Therefore, the working principle of the device can be summarised as follows: a change in temperature causes a change in shape and consequently also a change in the stress of the SMA wires. Particularly, when the wires are heated, they change their phase from DM to AU, which means that they recover their initial shape (see Figure 1) and thus their length decreases. This causes the spring to stretch and the axial load to increase. Conversely, when the wires are cooled from AU to DM, their length increases and thus the springs shorten and the axial load decreases. As mentioned, the changes of axial load induce changes of the adaptive TMD eigenfrequency (i.e. an increase in the axial load produces an increase in the eigenfrequency, while a decrease in the axial load produces a decrease in the eigenfrequency). This layout, which relies mainly on changes in the axial load of the wires rather than the change of their Young's moduli, allows the adaptive TMD eigenfrequency to change by more than 100% of the starting value, requires the use of low current values to heat the wires by means of Joule's effect, can be easily coupled to devices for adapting also the damping of the adaptive TMD, and does not require the SMA material used to have any special feature (Berardengo et al., 2015a). All these features make such a layout very attractive, and for this reason, this article further develops the concepts presented in Berardengo et al. (2015a) with the aim of developing a multi-modal adaptive TMD. As evidenced, the change of the axial load is obtained by heating (or cooling) the wires. Two physical phenomena determine the change of temperature of the wires: the Joule's effect and thermal convection (see the part related to the thermal model of the adaptive TMD, further in this article). These phenomena involve heat transfer, and thus, the adaptive TMD cannot change its eigenfrequency at high speed (e.g. changes in the eigenfrequency value equal to some Hertz in hundredths of a second). As an example, the specific adaptive TMD presented in the section of this article related to experiments is able to double its eigenfrequency (changes of about 10 or 15 Hz) in less than 10 s. Therefore, the adaptive TMDs proposed here can be taken into consideration in all those engineering applications where there is no need for high-speed changes of the device eigenfrequencies (e.g. when the eigenfrequencies of the primary system change because of thermal shifts). However, the bandwidth of such an adaptive TMD changes according to its design (e.g. SMA material, wire diameter, electric resistance of the SMA wires), and thus, the TMD can be built, to a certain extent, according to the specific application.

The main idea of this article is to design the adaptive TMD by using more than one mass (i.e. a number of masses equal to/higher than the number of the adaptive

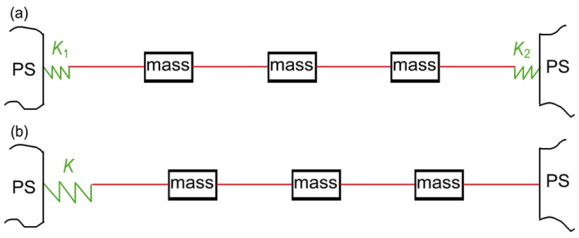

Figure 3. Layout of an SMA-based adaptive TMD with (a) three masses and its (b) equivalent scheme. Primary system abbreviated as PS in the figure.

TMD eigenfrequencies to be adapted; see Figure 3(a) as an example) connected to each other by an SMA wire and heating each wire independently from the others. Indeed, the eigenfrequency of the first m modes of an adaptive TMD with m masses (i.e. the modes which have significant eigenvector components at the degrees of freedom of the masses) can be changed in two different ways: by both changing the axial load, as already explained, and changing the TMD geometry. Both these effects are achieved when the SMA wire temperatures are changed.

Indeed, the increase/decrease in the axial load changes all the TMD eigenfrequencies at the same time, while heating the different wires independently can result in changes of the system geometry and thus of its eigenfrequencies. With this combined effect, the value of one eigenfrequency is not expected to be completely linked to the value of the others.

Consider, as an example, an adaptive TMD with three masses and four wires (see Figure 3(a)). In this case, the initial configuration at ambient temperature is assumed to be with all the wires of the same length. If the temperatures of the four wires are increased equally, the length of all the wires decreases by the same quantity and the axial load on the SMA wires increases, with a consequent increase in the values of all the first three eigenfrequencies. Instead, if the temperature of the first wire (i.e. the one between the left constraint and the adjacent mass) is increased more than the temperature of the other three wires, the length of the first wire decreases more than the length of the other wires. This implies an additional effect besides the increase in axial load: the change in the geometry of the adaptive TMD (i.e. the distance between the left constraint and the first mass decreases, in percentage, more than the distance between the first and the second masses, the distance between the second and the third masses and the distance between the third mass and the right constraint).

These two effects (i.e. change of axial load and change of geometry) are expected to enable the adaptation of different adaptive TMD eigenfrequencies with a certain level of independence. One of the targets of this article is to show that the mentioned principle actually works and is reliable.

It is important to recall that the discussion, as well as the results presented in this article, can be extended, without losing generality, to a device with more wires and masses able to adapt more eigenfrequencies. Therefore, the main goal of this article is to demonstrate that the special features of SMA materials make it possible to design and build adaptive TMDs capable of following the changes of (at least) two eigenfrequencies of the primary system at the same time.

Another aspect is worth being underlined: the proposed layout of the adaptive TMD can be easily coupled to devices able to adapt the damping as well, allowing for a fully adaptive device. This is one of the main features of the proposed adaptive TMD. As an example, an eddy current damper was coupled to the adaptive TMD of Figure 2 in Berardengo et al. (2015a), in order to adapt its damping. Several experimental tests showed that the TMD was fully adaptive and thus able to change both its eigenfrequency and its damping. Actually, also other principles could also be used in place of eddy currents. Since the possibility of changing the damping was already treated in the mentioned paper, and a possible solution was already validated, this work is focused just on the possibility of adapting eigenfrequencies.

The following section describes the analytical model of the multi-modal adaptive TMD needed to study the behaviour of the new proposed system.

Model of the multi-modal adaptive TMD

The model of the adaptive TMD must describe its eigenfrequencies (and mode shapes) as a function of the current flowing in the wires. To do so, three models are needed: (1) a thermal model which describes the temperature of the wires as a function of the flowing current (which is set by a user/controller), (2) a model of the material describing the stress value acting on the wires starting from their temperatures and (3) a dynamic model describing the eigenfrequencies and mode shapes as a function of the stress acting on the wires and of the mechanical and geometrical features of the adaptive TMD. The three models are described in the next subsections.

Thermal model

In the steady state, the power balance of each wire of the adaptive TMD is described by the following equation

$$s_{\mathrm{w,ext}} h (T - T_0) = R_{\mathrm{w}} i_{\mathrm{w}}^2 \tag{2}$$

where R_{w} is the electric resistance of the wire, i_{w} is the current flowing in the wire, h is the convection coefficient of air, T is the temperature of the wire, T_0 is the environmental temperature and $s_{\mathrm{w,ext}}$ is the outer surface of the wire. The expression of T as a function of i_{w} is achieved by rearranging equation (2)

$$T = \frac{R_{\mathrm{w}} i_{\mathrm{w}}^2}{h s_{\mathrm{w,ext}}} + T_0 \tag{3}$$

This model also evidences that the wire heats increasing the current flowing into it and thus exploiting the Joule's effect, while cooling is achieved by reducing the flowing current and exploiting the convection effect.

Material model

The model proposed here relies on the experimentally based one-dimensional (1D) material model (Lagoudas, 2008), then refined in Berardengo et al. (2015a) to take into account partial transformations. The hypotheses of the model are listed below, and they have already been shown to be appropriate for this work in Berardengo et al. (2015a):

- Young's modulus of the SMA material E_{w} is linearly dependent on the martensite volume fraction ξ ($\xi = 0$ when the material is fully austenitic and $\xi = 1$ when it is fully martensitic)

$$E_{\mathrm{w}} = E_{\mathrm{w,AU}} - \xi (E_{\mathrm{w,AU}} - E_{\mathrm{w,DM}}) \tag{4}$$

- The thermal expansion coefficient α is constant;
- The transformation strain linearly depends on ξ

$$\varepsilon_{\mathrm{w}}^{\mathrm{t}} = \xi H^{\mathrm{cur}} \tag{5}$$

- The start and end transformation temperatures at non-null stress (i.e. $M_{\mathrm{s}}^{\sigma}, M_{\mathrm{f}}^{\sigma}, A_{\mathrm{s}}^{\sigma}, A_{\mathrm{f}}^{\sigma}$) linearly depend on σ_{w}

$$\begin{aligned} M_{\mathrm{s}}^{\sigma} &= M_{\mathrm{s}} + \frac{\sigma_{\mathrm{w}}}{C_{\mathrm{M}}}, M_{\mathrm{f}}^{\sigma} = M_{\mathrm{f}} + \frac{\sigma_{\mathrm{w}}}{C_{\mathrm{M}}}, \\ A_{\mathrm{s}}^{\sigma} &= A_{\mathrm{s}} + \frac{\sigma_{\mathrm{w}}}{C_{\mathrm{A}}}, A_{\mathrm{f}}^{\sigma} = A_{\mathrm{f}} + \frac{\sigma_{\mathrm{w}}}{C_{\mathrm{A}}} \end{aligned} \tag{6}$$

- During transformations from DM to AU (i.e. increase in the temperature, $\dot{T} > 0$, or decrease in the stress applied to the wire, $\dot{\sigma}_{\mathrm{w}} < 0$; the dot indicates the first derivative with respect to time t), ξ is

$$\xi = \begin{cases} \xi_{-1}, T \leqslant A_{\mathrm{s}}^{\sigma} \\ \dfrac{A_{\mathrm{f}}^{\sigma} - T}{A_{\mathrm{f}} - A_{\mathrm{s}}} \xi_{-1}, A_{\mathrm{s}}^{\sigma} < T < A_{\mathrm{f}}^{\sigma} \\ 0, T \geqslant A_{\mathrm{f}}^{\sigma} \end{cases} \tag{7}$$

where ξ_{-1} is the martensite volume fraction at the beginning of the transformation.

- During transformations from AU to DM (i.e. decrease in the temperature, $\dot{T}<0$, or increase in the stress applied to the wire, $\dot{\sigma}_{\mathrm{w}}>0$), ξ is

$$\xi = \begin{cases} \xi_{-1}, T \geqslant M_{\mathrm{s}}^{\sigma} \\ \dfrac{M_{\mathrm{s}}^{\sigma} - T}{M_{\mathrm{s}} - M_{\mathrm{f}}}(1 - \xi_{-1}) + \xi_{-1}, M_{\mathrm{f}}^{\sigma} < T < M_{\mathrm{s}}^{\sigma} \\ 1, T \leqslant M_{\mathrm{f}}^{\sigma} \end{cases} \quad (8)$$

Using equations (4), (5) and (1), the length L_{wh}^{r} of the rth wire (the variables related to the rth wire will be indicated by the superscript r from here on) of the adaptive TMD strained by the force F produced by the spring (without considering any other static or dynamic load) can be written as

$$L_{\mathrm{wh}}^{\mathrm{r}} = \left(1 + \varepsilon_{\mathrm{w}}^{\mathrm{r}}\right) L_{\mathrm{w}}^{\mathrm{r}} = \left[1 + \frac{\sigma_{\mathrm{w}}^{\mathrm{r}}}{E_{\mathrm{w,AU}} - \xi^{\mathrm{r}}\left(E_{\mathrm{w,AU}} - E_{\mathrm{w,DM}}\right)} + \xi^{\mathrm{r}} H^{\mathrm{cur},r} + \alpha^{\mathrm{r}}\left(T - T_0\right)\right] L_{\mathrm{w}}^{\mathrm{r}} \quad (9)$$

where $L_{\mathrm{w}}^{\mathrm{r}}$ is the unstrained length of the rth wire.

Since the layout of the new proposed adaptive TMD alternates SMA wires and masses (as shown in Figure 3(a) for a device with three masses), it is possible to state that $\sigma_{\mathrm{w}}^{1} = \sigma_{\mathrm{w}}^{2} = \cdots = \sigma_{\mathrm{w}}^{n}$, where n is the number of wires of the adaptive TMD (the number of masses is $n - 1$). Therefore, the same stress value (indicated as σ_{w}) acts on all the wires.

In order to obtain a simpler analytical model, the layout of Figure 3(a) is now modelled as shown in Figure 3(b), where the two springs of Figure 3(a) have been modelled as a single spring, whose stiffness K is calculated considering the series of the two springs of Figure 3(a) and their stiffness values (i.e. K_1 and K_2). More details about the way to set the value of K can be found in Berardengo et al. (2015a). Furthermore, and for the sake of simplicity, the wires are assumed to be made from the same SMA material, which in turn means that $\alpha^{1} = \alpha^{2} = \cdots = \alpha^{\mathrm{n}} = \alpha$ and $H^{\mathrm{cur},1} = H^{\mathrm{cur},2} = \cdots = H^{\mathrm{cur,n}} = H^{\mathrm{cur}}$. However, this assumption does not cause any loss of generality of the mathematical treatment.

According to Figure 4, the following relation holds between the displacement of the outer end of the SMA wire u and the stretch of the spring q

$$u = -q \quad (10)$$

Figure 4. Scheme of the device.

If the axial load F is changed from a situation of equilibrium (i.e. from F_{old} to F_{new}, $F_{\mathrm{new}} - F_{\mathrm{old}} = \bar{\Delta}F$), then u and q are non-null quantities and the stress σ_{w} changes (i.e. $\bar{\Delta}\sigma_{\mathrm{w}} = \sigma_{\mathrm{w,new}} - \sigma_{\mathrm{w,old}}$), as well as the strain (i.e. $\bar{\Delta}\varepsilon_{\mathrm{w}} = \varepsilon_{\mathrm{w,new}} - \varepsilon_{\mathrm{w,old}}$). Vice versa, if a $\bar{\Delta}\varepsilon_{\mathrm{w}}$ occurs, the axial force F changes as well. According to equation (10) and the central term of equation (9)

$$\bar{\Delta}F = \bar{\Delta}\sigma_{\mathrm{w}} A_{\mathrm{w}} = Kq = -Ku = -K\sum_{r=1}^{n}\left(\bar{\Delta}\varepsilon_{\mathrm{w}}^{\mathrm{r}} L_{\mathrm{w}}^{\mathrm{r}}\right) \quad (11)$$

where A_{w} is the cross section of the wires (equation (11) assumes the same value of A_{w} for all the wires). It should be noted that the change of A_{w} due to strain can be neglected for the purpose of this article (Berardengo et al., 2015a).

Then, according to the right-hand term of equation (9), equation (11) can be rearranged as

$$\begin{aligned} & -A_{\mathrm{w}}\frac{\left(\sigma_{\mathrm{w,new}} - \sigma_{\mathrm{w,old}}\right)}{K} \\ & = \sum_{r=1}^{n}\left\{\left[\frac{\sigma_{\mathrm{w,new}}}{E_{\mathrm{w,AU}} - \xi_{\mathrm{new}}^{\mathrm{r}}\left(E_{\mathrm{w,AU}} - E_{\mathrm{w,DM}}\right)} - \frac{\sigma_{\mathrm{w,old}}}{E_{\mathrm{w,old}}^{\mathrm{r}}} + \alpha\left(T_{\mathrm{new}}^{\mathrm{r}} - T_{\mathrm{old}}^{\mathrm{r}}\right) + \left(\xi_{\mathrm{new}}^{\mathrm{r}} - \xi_{\mathrm{old}}^{\mathrm{r}}\right) H^{\mathrm{cur}}\right] L_{\mathrm{w}}^{\mathrm{r}}\right\} \end{aligned} \quad (12)$$

This equation can be used to simulate the behaviour of the wires from a known reference condition, for example, the initial condition where no current flows into the wires and thus their temperature is equal to T_0. If the change of configuration is achieved by changing the current flowing into the wires, equation (3) can be used to estimate $T_{\mathrm{new}}^{\mathrm{r}}$, once a given current value is set for each wire. Therefore, the only unknowns of equation (12) are $\sigma_{\mathrm{w,new}}$ and $\xi_{\mathrm{new}}^{\mathrm{r}}$. This latter variable ($\xi_{\mathrm{new}}^{\mathrm{r}}$) can be written as a function of $\sigma_{\mathrm{w,new}}$ for each wire, using either equation (7) or equation (8), according to the transformation faced by the considered wire. Finally, the only unknown of equation (12) is $\sigma_{\mathrm{w,new}}$, which can then be derived. Finally, $L_{\mathrm{wh}}^{\mathrm{r}}$ can be estimated by means of equation (9), and F can be found as $\sigma_{\mathrm{w,new}} A_{\mathrm{w}}$. This new configuration then becomes the reference configuration when the flowing currents are changed by the user and the new wire lengths and axial load must be estimated.

Dynamic model

The value of the length of the wires and the stress acting on the wires affect the value of the eigenfrequencies of the adaptive TMD, as already mentioned. The aim of this subsection is to provide a way to calculate the eigenfrequencies by knowing $\sigma_{w,\,new}$ and L^{r}_{wh}.

The hypotheses of the approach used in this section are the following (Cheli and Diana, 2015):

- The wires are considered as strings. Shear force and bending moment are thus neglected;
- Each string is made of homogeneous material, and its characteristics do not change with space and time (when the values of the currents flowing into the wires are constant);
- Each string has constant cross section in space and time;
- The mass per unit length is constant along the string;
- The axial tension F of the string is high with respect to the adaptive TMD weight. Consequently, the adaptive TMD configuration can be approximated as rectilinear in the static equilibrium position. This hypothesis is always well approximated in the numerical/experimental applications discussed in this article (see further on);
- The amplitude of the vibration of the masses of the adaptive TMD is limited. This implies that geometric non-linearity can be neglected and variations of the axial load acting on the wires due to the transversal vibration of the string are negligible if compared to the value of F in the static configuration (i.e. the value which can be estimated by means of the model of the previous subsection). This hypothesis is usually verified when random vibrations (due to random disturbances) are taken into consideration, which is a common practical case. However, the model presented here is the base for a possible development in the treatment of harmonic disturbances with higher vibration levels where, consequently, geometric non-linearity and variations of the axial load acting on the wires due to the transversal vibration of the string (which could cause SMA phase changes) must be taken into account. From here on, the case of low vibration amplitudes will be considered, and therefore, geometric non-linearity and variations of the axial load acting on the wires due to the transversal vibration of the string will be neglected. This can be seen as equivalent to considering the case of either random vibrations (as in the experiments presented further in the manuscript) or low-amplitude harmonic vibrations;
- The axial tension is assumed to be constant in space and time (when the values of the currents flowing into the wires are constant);
- Damping is neglected;
- The masses of the adaptive TMD are concentrated masses. In practical cases, this means that their size must be small if compared to the length of the whole adaptive TMD. However, this hypothesis is used here just for the sake of simplicity and it could be removed if necessary.

Relying on these hypotheses, which are more than reasonable for the presented device, and considering an infinitesimal portion of string (see Figure 5), the following equilibrium in the vertical direction, with respect to the static configuration of the string, can be written as

$$-F_{in} + F\sin(\alpha_R) - F\sin(\alpha_L) = 0 \qquad (13)$$

Referring to Figure 5 and equation (13), $w(x,\,t)$ is the vertical displacement of the string evaluated at time t and in correspondence of the string section located at a distance x from the left extremity. F, the axial tension of the string, is always perpendicular to the string cross section. The angles α_L and α_R are the left and right angles that the deformed infinitesimal piece of string forms with the horizontal plane during vibrations, respectively.

Finally, F_{in} is the inertial force acting on the infinitesimal piece of the string, which can be rewritten as the product between its mass (i.e. $m_d dx$, where m_d is the mass per unit length) and its acceleration

$$F_{in} = m_d dx \frac{\partial^2 w}{\partial t^2} \qquad (14)$$

Thanks to the hypothesis of small vibration amplitudes, the following approximations are valid (Cheli and Diana, 2015)

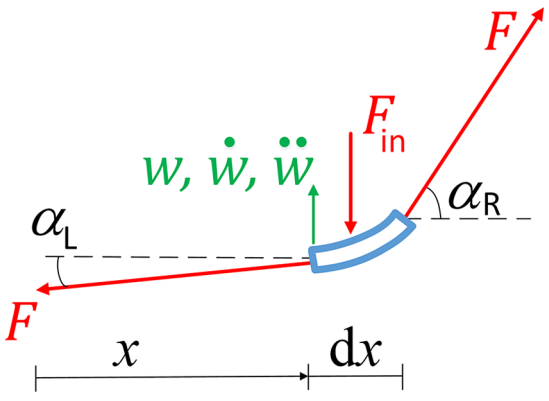

Figure 5. Forces acting on an infinitesimal portion of tensioned string.

$$\sin(\alpha_L) \simeq \alpha_L \simeq \tan(\alpha_L) = \frac{\partial w}{\partial x},$$
$$\sin(\alpha_R) \simeq \alpha_R \simeq \tan(\alpha_R) = \frac{\partial}{\partial x}\left(w + \frac{\partial w}{\partial x}dx\right) \quad (15)$$

Substituting equations (14) and (15) into equation (13), the following expression is obtained

$$m_d \frac{\partial^2 w}{\partial t^2} = F \frac{\partial^2 w}{\partial x^2} \quad (16)$$

This partial differential equation leads to the following expression of $w(x, t)$ (Cheli and Diana, 2015; i.e. general expression of the standing wave solution)

$$w(x,t) = \left[Z \sin\left(x\omega\sqrt{\frac{m_d}{F}}\right) + P \cos\left(x\omega\sqrt{\frac{m_d}{F}}\right)\right] \cos(\omega t + \theta) \quad (17)$$

where ω is the angular frequency and θ is a constant.

The natural frequencies and the mode shapes (depending on the constants Z and P) are functions of the boundary conditions.

The spatial function in equation (17) (named here as $\Phi(x)$) is

$$\Phi(x) = \left[Z \sin\left(x\omega\sqrt{\frac{m_d}{F}}\right) + P \cos\left(x\omega\sqrt{\frac{m_d}{F}}\right)\right] \quad (18)$$

Equation (18) is valid for strings without any discontinuity. Since the adaptive TMD is made with more than one wire, equation (18) must be written for each of them. The boundary conditions related to all the wires must also be written, taking into account that the natural frequencies are the same for all of them, because they are part of the same dynamical system.

As an example, consider an adaptive TMD made from two masses (M_1 and M_2) and three wires. Equation (18) is rewritten as three different equations, and there are six unknowns to be found imposing the boundary conditions: Z_1, P_1, Z_2, P_2, Z_3 and P_3. Indeed, referring to the coordinate along the first wire as x_1 (with $0 \leqslant x_1 \leqslant L^1_{wh}$), the one along the second wire as x_2 (with $0 \leqslant x_2 \leqslant L^2_{wh}$) and the one along the third wire as x_3 (with $0 \leqslant x_3 \leqslant L^3_{wh}$), the mentioned three equations are obtained (in this case, the three wires are considered as having the same value of m_d, and the changes in m_d due to strains are considered negligible)

$$\Phi(x_1) = \left[Z_1 \sin\left(x_1\omega\sqrt{\frac{m_d}{F}}\right) + P_1 \cos\left(x_1\omega\sqrt{\frac{m_d}{F}}\right)\right] \quad (19)$$

$$\Phi(x_2) = \left[Z_2 \sin\left(x_2\omega\sqrt{\frac{m_d}{F}}\right) + P_2 \cos\left(x_2\omega\sqrt{\frac{m_d}{F}}\right)\right] \quad (20)$$

$$\Phi(x_3) = \left[Z_3 \sin\left(x_3\omega\sqrt{\frac{m_d}{F}}\right) + P_3 \cos\left(x_3\omega\sqrt{\frac{m_d}{F}}\right)\right] \quad (21)$$

The system of equations coming from the application of all the boundary conditions makes it possible to find the eigenfrequencies of the adaptive TMD as well as the mode shapes. Two boundary conditions are given by the constraints between the adaptive TMD and the primary system (i.e. pinned–pinned condition in this case). Two further conditions (or more in case a layout with more than two masses is considered) are given by the vertical dynamic equilibria of the two masses of the adaptive TMD. Finally, the two remaining conditions (or more in case a layout with more than two masses is taken into account) are provided by the imposition of the same vertical displacement for consecutive outer points of wires (e.g. the last point of the first wire and the first point of the second wire; indeed, concentrated masses are considered here).

Recalling the hypotheses of small amplitudes of vibration and the fact that concentrated masses are taken into account, the above-mentioned boundary conditions are written as (Gómez et al., 2007)

$$\Phi(x_1 = 0) = 0 \quad (22)$$

$$\Phi\left(x_3 = L^3_{wh}\right) = 0 \quad (23)$$

$$F\left(\left.\frac{\partial w}{\partial x_2}\right|_{x_2=0} - \left.\frac{\partial w}{\partial x_1}\right|_{x_1=L^1_{wh}}\right) = M_1 \left.\frac{\partial^2 w}{\partial t^2}\right|_{x_2=0}$$
$$\Rightarrow F\left(\left.\frac{d\Phi}{dx_2}\right|_{x_2=0} - \left.\frac{d\Phi}{dx_1}\right|_{x_1=L^1_{wh}}\right) = -\omega^2 M_1 \Phi(x_2 = 0) \quad (24)$$

$$F\left(\left.\frac{\partial w}{\partial x_3}\right|_{x_3=0} - \left.\frac{\partial w}{\partial x_2}\right|_{x_2=L^2_{wh}}\right) = M_2 \left.\frac{\partial^2 w}{\partial t^2}\right|_{x_3=0}$$
$$\Rightarrow F\left(\left.\frac{d\Phi}{dx_3}\right|_{x_3=0} - \left.\frac{d\Phi}{dx_2}\right|_{x_2=L^2_{wh}}\right) = -\omega^2 M_2 \Phi(x_3 = 0) \quad (25)$$

$$\Phi\left(x_1 = L^1_{wh}\right) = \Phi(x_2 = 0) \quad (26)$$

$$\Phi\left(x_2 = L^2_{wh}\right) = \Phi(x_3 = 0) \quad (27)$$

In this case, the following matrix equation is obtained

$$\begin{bmatrix} 0 & 1 & 0 & 0 & 0 & 0 \\ \sin(\gamma L^1_{wh}) & \cos(\gamma L^1_{wh}) & 0 & -1 & 0 & 0 \\ -F\gamma\cos(\gamma L^1_{wh}) & F\gamma\sin(\gamma L^1_{wh}) & F\gamma & M_1\omega^2 & 0 & 0 \\ 0 & 0 & \sin(\gamma L^2_{wh}) & \cos(\gamma L^2_{wh}) & 0 & -1 \\ 0 & 0 & -F\gamma\cos(\gamma L^2_{wh}) & F\gamma\sin(\gamma L^2_{wh}) & F\gamma & M_2\omega^2 \\ 0 & 0 & 0 & 0 & \sin(\gamma L^3_{wh}) & \cos(\gamma L^3_{wh}) \end{bmatrix} \begin{bmatrix} Z_1 \\ P_1 \\ Z_2 \\ P_2 \\ Z_3 \\ P_3 \end{bmatrix} = \begin{bmatrix} 0 \\ 0 \\ 0 \\ 0 \\ 0 \\ 0 \end{bmatrix} \quad (28)$$

where $\gamma = \omega\sqrt{m_d/F}$

The values of the eigenfrequencies are yielded by solving the following equation with respect to ω (Cheli and Diana, 2015)

$$\det \begin{bmatrix} 0 & 1 & 0 & 0 & 0 & 0 \\ \sin(\gamma L^1_{wh}) & \cos(\gamma L^1_{wh}) & 0 & -1 & 0 & 0 \\ -F\gamma\cos(\gamma L^1_{wh}) & F\gamma\sin(\gamma L^1_{wh}) & F\gamma & M_1\omega^2 & 0 & 0 \\ 0 & 0 & \sin(\gamma L^2_{wh}) & \cos(\gamma L^2_{wh}) & 0 & -1 \\ 0 & 0 & -F\gamma\cos(\gamma L^2_{wh}) & F\gamma\sin(\gamma L^2_{wh}) & F\gamma & M_2\omega^2 \\ 0 & 0 & 0 & 0 & \sin(\gamma L^3_{wh}) & \cos(\gamma L^3_{wh}) \end{bmatrix} = 0 \quad (29)$$

The values ω_i, which are solutions of equation (29), are the eigenfrequencies of the adaptive TMD (ω_i will indicate the ith eigenfrequency from here on). The mode shape corresponding to each ω_i can be calculated by first substituting the value of ω_i into equation (28) and finding the unknown constants Z and P (actually, one of these constants needs to be arbitrarily set to a given value because one scalar equation of the matrix equation (28) is linearly dependent on the other scalar equations due to the condition imposed through equation (29)) and then substituting the values of these constants and the value of ω_i into equations (19) to (21).

The presented method can be applied to calculate the eigenfrequencies and mode shapes of the adaptive TMD (see Figure 6 as an example), once the values of F and L^r_{wh} are known (see the previous subsection). Therefore, the three models described here (i.e. thermal model, material model and dynamic model) can be used to calculate the adaptive TMD eigenfrequencies as functions of its inputs, which are the currents flowing into the SMA wires.

This global model will be used in the following section to study the possibility of designing multi-modal adaptive TMDs where it is possible to adapt different eigenfrequencies independently.

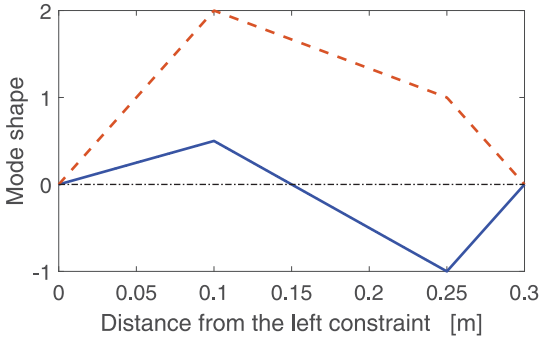

Figure 6. The first two mode shapes for an adaptive TMD with two masses of 100 g and a total length of 30 cm. The first mass is 10 cm from the left constraint, and the second one 25 cm. The black dash-dotted line represents the undeformed configuration, the red dashed line the first mode (at about 5.8 Hz), and the blue solid line the second mode (at about 8.7 Hz).

System analysis

The models presented previously are now used to study the behaviour of a multi-modal adaptive TMD. There are two points which must be taken into account:

1. The first is how to set the initial configuration of the adaptive TMD (i.e. starting values of its natural frequencies) through a change in the initial geometry and layout. This means that the study is finalized to understand how the first eigenfrequencies (i.e. those where the masses of the adaptive TMD show significant displacements: the first two modes for an adaptive TMD with two masses, the first three modes for an adaptive TMD with three masses, etc.) change, changing the length of the whole adaptive TMD, the length of each wire (and thus the position of each mass) and the weight of each mass.
2. Once the initial configuration is set (as explained in the previous point), the second analysis is aimed at understanding if (and how much) it is possible to change one eigenfrequency independently from the others. This point is related to the capability of the adaptive TMD to follow the changes of different eigenfrequencies of the primary system.

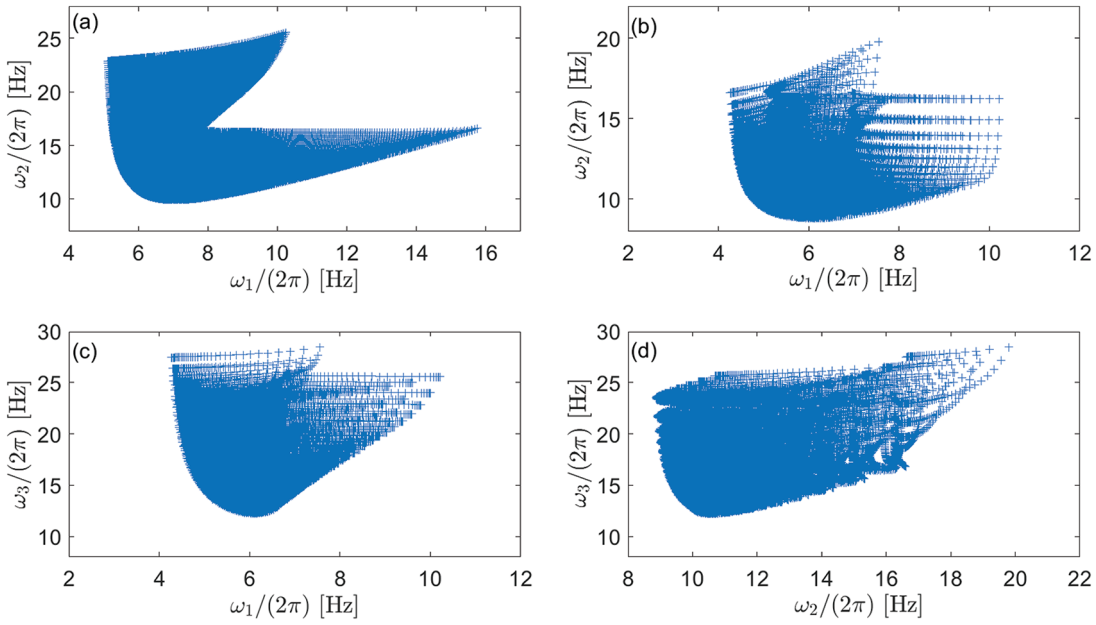

Figure 7. Eigenfrequency configurations achieved by changing the initial adaptive TMD layout at environmental temperature (adaptive TMD with a length of 20 cm and masses of 100 g): (a) adaptive TMD with two masses and (b, c and d) adaptive TMD with three masses.

These two points are treated in the next two subsections.

The value of K used in the next simulations was set in order to have a stress acting on the wires equal to 50 MPa at ambient temperature with all the wires in DM (indeed, this stress value is higher than σ_f for the material used in the experimental tests) and to 200 MPa with all the wires in AU, thus having heated the wires (this stress value is lower than the full scale suggested by the manufacturer for the material used in the experiments, that is, 250 MPa).

Set of the initial configuration

The aim of this section is to show that a change in the initial geometry of the adaptive TMD (i.e. the length of the whole adaptive TMD, the length of each wire, and thus the position of each mass, and the weight of each mass) allows the user to set the first eigenfrequencies of the adaptive TMD in a wide frequency range. At first, an adaptive TMD with two masses is discussed, and then, three masses are taken into account. The dynamic model discussed previously was used to perform the simulations, which were carried out on an adaptive TMD chosen as an example, having at first a total length of 20 cm and masses of 100 g.

Among the various parameters that can be adjusted to set the initial configuration of the adaptive TMD, the effects of the mass values, the total length of the adaptive TMD and the initial stress σ_w are known (e.g. Cheli and Diana, 2015; Meirovitch, 2001): they shift the adaptive TMD natural frequencies. Therefore, the analyses focused on the effects of the mass ratio and the length of the wires. Initially, the mass ratio of the adaptive TMD was kept constant (both the masses with equal mass, and thus, ratio equal to 1) and just the effect of the mass locations was studied. After this, the influence of the mass ratio on the results was investigated. Therefore, at first, the location of the masses was changed step by step of 0.1% of the total length of the adaptive TMD, assuring that the distance between the two masses and the distance between one mass and the closest constraint were always higher than or equal to 5% of the total length of the adaptive TMD. The simulations were carried out at environmental temperature (i.e. $\sigma_w = 50$ MPa). The plot obtained for the adaptive TMD with two masses is shown in Figure 7(a). It is evident that the two eigenfrequencies cover a wide frequency range.

Figures 7(b) to (d) instead show the trend of the first three eigenfrequencies for an adaptive TMD with three masses. This time the step used to change the position of the masses was 1% in order to decrease the computational burden of the simulations. In plots (b), (c) and (d), there are some blank spaces, which are due to the step used (i.e. 1%). A narrower step would allow these spaces to be filled in, which means that the envelope of the points must be considered for a detailed analysis of all the possible initial eigenfrequencies that can be obtained with this configuration.

If the primary system eigenfrequencies to be controlled are out of the shown working areas, it is possible, as mentioned, to act on the total length of the

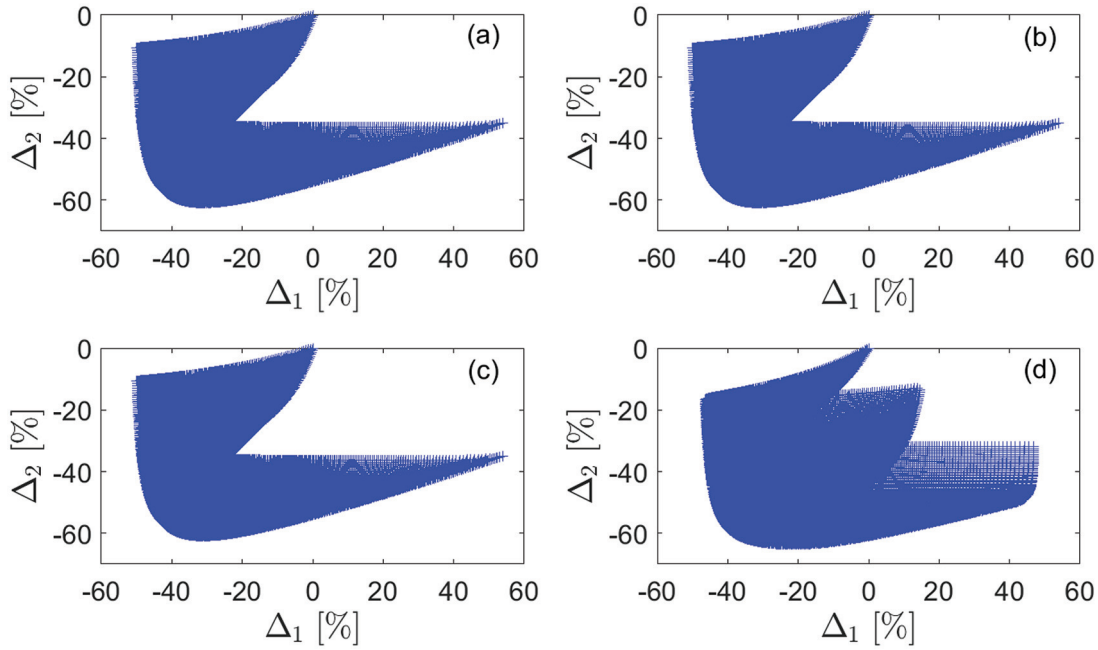

Figure 8. Percentage changes Δ of the first two eigenfrequencies for an adaptive TMD with two masses: (a) length of 20 cm and masses of 100 g, (b) length of 40 cm and masses of 100 g, (c) length of 20 cm and masses of 200 g and (d) length of 20 cm and one mass of 100 g and the other equal to 200 g.

adaptive TMD and/or the mass values in order to shift the envelopes. Other possibilities are to increase either the value of σ_w at the environmental temperature or the number of the masses of the adaptive TMD.

An interesting aspect can be noticed looking at Figures 8(a) to (c), where the percentage variations Δ of the adaptive TMD eigenfrequencies are presented for different layouts of an adaptive TMD with two masses. Here, Δ is evaluated considering the reference frequency value obtained when the masses are as close as possible to their left constraint. From the simulations, it appears that the Δ values are not dependent on the mass values (for equal masses) or the total length (compare Figures 8(a) to (c) as an example, where doubling the adaptive TMD length or the mass values does not change the plot points). In order to widen the percentage variation of the eigenfrequencies, it is possible to act on the mass ratio. Indeed, its effect can be used to extend the envelope of the graphs, thus increasing the possible frequency combinations which can be obtained, as can be noticed by comparing Figure 8(a) and (d).

This analysis has shown that the initial values of the adaptive TMD eigenfrequencies can be easily set by acting on the device geometry and that wide frequency ranges can be covered. As a consequence, the initial eigenfrequencies of the adaptive TMD can be tuned with the initial values of the primary system eigenfrequencies to be damped. The next section takes into account the second key analysis listed previously: the capability of the adaptive TMD to change its eigenfrequencies independently by heating its different wires separately.

Adaptation capability

This section shows how the eigenfrequencies of the adaptive TMD change by changing the temperatures of the wires. In theory, the current i_w should be changed, which would cause a temperature change. However, since there is just one constant between the square of the current and the change of the temperature of each wire (see equation (3)), the temperature was used directly as input in this numerical analysis. The procedure followed for the simulations is explained here for an adaptive TMD with two masses for the sake of simplicity. It was, however, also used for the adaptive TMD with three masses discussed further in this subsection.

To evaluate the behaviour of the adaptive TMD, the temperatures of the three wires were initially set at the environmental temperature and $\sigma_w = 50$ MPa. The material model and the dynamic model (shown earlier in this article) were used to find the first two eigenfrequencies of the adaptive TMD. Then, the temperature of the first wire was increased by 2 °C and the eigenfrequencies were calculated again. The temperature of the first wire was then changed step by step by 2 °C up to 120 °C. This last temperature is higher than 103.91 °C, which is the temperature at which the wires complete the transformation in AU at a stress value of 200 MPa (which is the maximum target stress in these simulations, as mentioned previously). The temperature of the wire was then decreased again to the environmental temperature in steps of 2 °C. At each step, the adaptive TMD eigenfrequencies were calculated.

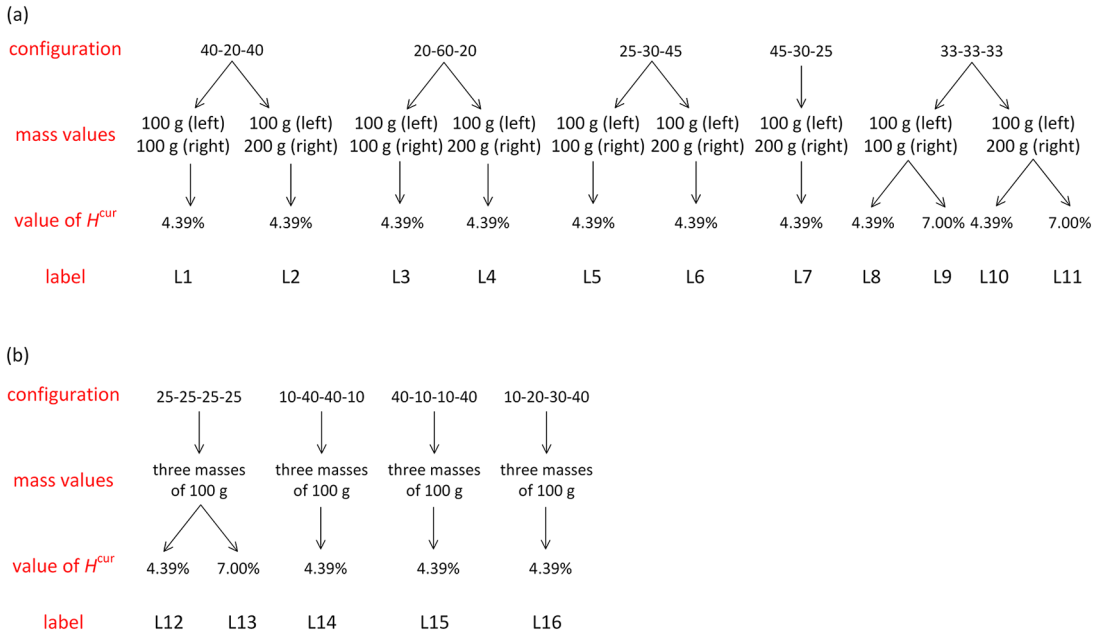

Figure 9. Layouts tested numerically for an adaptive TMD with (a) two masses and (b) three masses and the corresponding labels.

After this cycle, the temperature of the second wire was increased by 2 °C, and the cycle for the temperature of the first wire repeated. When also the second wire had completed the temperature cycle (i.e. the second wire was finally cooled again to ambient temperature), the temperature of the third wire was changed by 2 °C and the previous procedure repeated. The simulations ended when also the third wire had completed a temperature cycle.

A simulation of this kind makes it possible to build the envelope of stress–temperature points which can be described by the adaptive TMD and thus to describe all the possible combinations of the values of the first two eigenfrequencies of the adaptive TMD. It is noticed that when a wire is heated/cooled, phase transformation can also occur in the other wires, even if they are at constant temperature. Indeed, a change of temperature in a wire causes a change of the applied stress in all the wires at the same time. Therefore, the wires at constant temperature could experience pseudoelastic-induced phase transitions (see Figure 1).

Before discussing the results, it is worth explaining that some specific layouts, chosen as examples, were taken into consideration for this study. Figure 9(a) presents the cases considered for an adaptive TMD with two masses, while Figure 9(b) shows the cases considered for an adaptive TMD with three masses. Each TMD considered in the analysis has a specific label (see Figure 9) for a direct reference.

The initial geometrical configuration for the adaptive TMDs of Figure 9 is indicated with three numbers. As an example, the configuration 25-30-45 indicates that the first wire has a length equal to 25% of the total length of the adaptive TMD, the second wire (i.e. the central wire) has a length equal to 30%, and the third wire to 45% of the total length of the adaptive TMD.

Figure 10 shows the resulting percentage plot for different adaptive TMD configurations. Here, the symbol Θ is used to indicate the percentage change of the eigenfrequencies. Previously, the same quantity was indicated as Δ. These different symbols allow the recognition of the reason for the eigenfrequency change: Δ indicates an eigenfrequency change at environmental temperature due to a change in the adaptive TMD configuration (e.g. a change in the initial distance between two masses), while Θ indicates a change due to a change in the wire temperature (and thus in the current flowing into a wire). The reference values for calculating the percentage values are the eigenfrequency values with all the wires at environmental temperature in DM. This type of plot will be named percentage adaptation plot (PAP) from here on. It is noticed that the PAP is neither a function of the global length of the adaptive TMD nor of the mass values (for equal masses). As examples, if the global length of the adaptive TMD used in Figure 10(a) is doubled and/or the masses used are doubled, the resulting PAP does not change.

From Figure 10, it can be seen that the maximum possible change of the eigenfrequencies is about 104%, and the plots have a mean slope that is almost unitary. The blank spaces among points are again due to the step used in the simulations (i.e. 2 °C). A smaller step would fill in these spaces.

It is evident that for a given value of the first eigenfrequency, more than one value of the second eigenfrequency can be achieved and vice versa. This

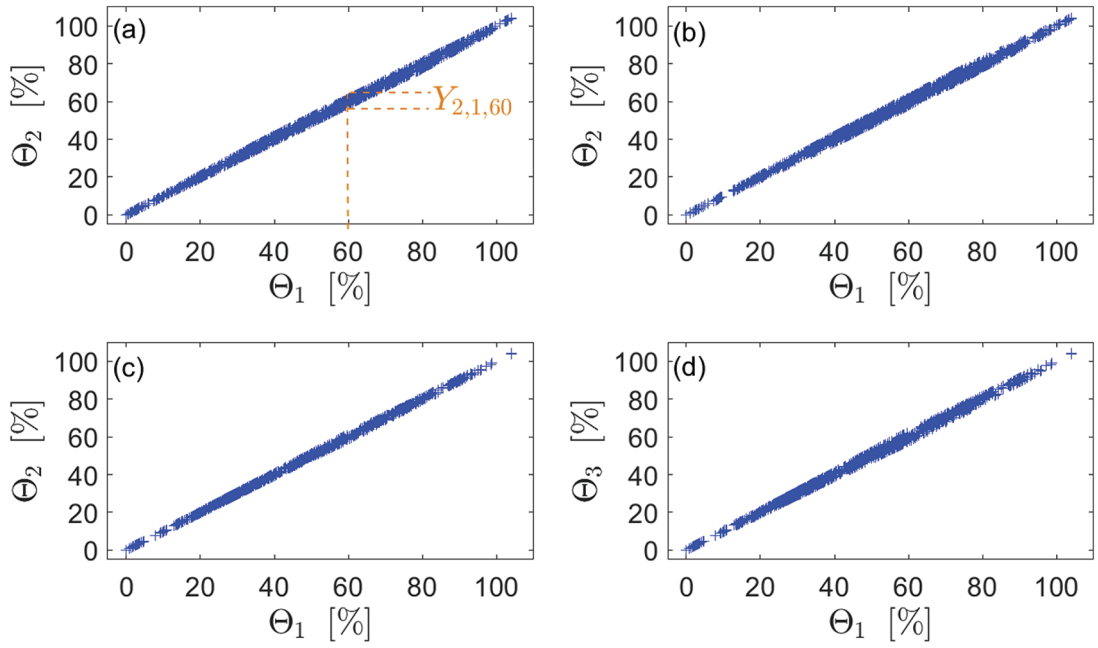

Figure 10. Adaptation plots for different adaptive TMD configurations: (a) two masses of 100 g with a global length of 20 cm and a wire configuration 25-30-45 (L5, see Figure 9), (b) two masses (one equal to 100 g and the other to 200 g) with a global length of 40 cm and a wire configuration 33-33-33 (L10) and (c and d) three masses of 100 g with a global length of 40 cm and a wire configuration 25-25-25-25 (L12).

Table 2. Maximum possible spans of the second eigenfrequency as a function of the first eigenfrequency for different configurations of an adaptive TMD with two masses (with equal values) and three wires.

Percentage length of the three wires (left-central-right) as function of the total length of the adaptive TMD	$Y_{2,1,20}$	$Y_{2,1,60}$	$Y_{2,1,80}$	$Y_{2,1}^{\max}$
40-20-40 (L1, see Figure 9)	2.5%	3.2%	4.8%	4.9%
20-60-20 (L3)	0.5%	2.4%	1.8%	2.6%
25-30-45 (L5)	1.6%	3.4%	4.0%	4.3%
33-33-33 (L8)	1.2%	3.4%	3.3%	3.8%

TMD: tuned mass damper.
The test labels are those presented in Figure 9.

demonstrates the capability of the adaptive TMD to adapt two different eigenfrequencies separately. Obviously, full independence is not possible, but the extent of the frequency shift of a resonance when the other is fixed (i.e. the width of the plot) can be increased, as will be shown further in this section. Table 2 summarises the results related to the span of the second eigenfrequency as a function of the value of the first one for several cases presented in Figure 9(a) (TMDs with two masses). The symbol $Y_{z,g,v}$ used in this table indicates the maximum possible percentage change of the zth eigenfrequency for a given value of the gth eigenfrequency. As an example, $Y_{2,1,60}$ expresses the maximum possible percentage change of the second eigenfrequency by a value of the first eigenfrequency that is shifted by 60% compared to the reference value (see Figure 10(a)). Moreover, the maximum values of $Y_{\mathrm{z,g,v}}$ as a function of v will be referred to as $Y_{z,g}^{\max}$. In the cases of Figure 10, the value of H^{cur} was equal to that shown in Table 1 (which is that of the material used in the further experiments, that is, 4.39%). However, an SMA material with a higher value of H^{cur} (e.g. 7%, which is possible in practice) would significantly increase the resulting spans (compare the last row of Table 2 with Table 3 where the material data are those of Table 1, exception made for H^{cur} in Table 3).

Tables 2 and 3 are related to the case in which the two masses have the same value. Conversely, Table 4 refers to a case where different mass values are used (see also Figure 10(b)); the material data are again those of Table 1. Moreover, Table 5 shows the results for one configuration of Table 4 (i.e. 33-33-33) with $H^{\mathrm{cur}} = 7\%$.

Table 3. Maximum possible spans of the second eigenfrequency as a function of the first eigenfrequency of an adaptive TMD with two masses (with equal values) and three wires (H^{cur} = 7%).

Percentage length of the three wires (left-central-right) as function of the total length of the adaptive TMD	$Y_{2,1,20}$	$Y_{2,1,60}$	$Y_{2,1,80}$	$Y_{2,1}^{max}$
33-33-33 (L9)	1.9%	5.3%	5.8%	6.0%

TMD: tuned mass damper.
The test labels are those presented in Figure 9.

Table 4. Maximum possible spans of the second eigenfrequency as a function of the first eigenfrequency for different configurations of an adaptive TMD with two masses (with different values: the mass on the left is 100 g, while the other 200 g) and three wires.

Percentage length of the three wires (left-central-right) as function of the total length of the adaptive TMD	$Y_{2,1,20}$	$Y_{2,1,60}$	$Y_{2,1,80}$	$Y_{2,1}^{max}$
40-20-40 (L2)	2.0%	4.0%	3.3%	4.4%
20-60-20 (L4)	2.0%	4.2%	4.9%	4.9%
25-30-45 (L6)	1.0%	3.2%	2.2%	3.6%
33-33-33 (L10)	1.3%	3.6%	3.9%	4.4%
45-30-25 (L7)	1.7%	4.2%	4.9%	5.0%

TMD: tuned mass damper.
The test labels are those presented in Figure 9.

Table 5. Maximum possible spans of the second eigenfrequency as a function of the first eigenfrequency of an adaptive TMD with two masses (with different values: the mass on the left is 100 g, while the other 200 g) and three wires (H^{cur} = 7%).

Percentage length of the three wires (left-central-right) as function of the total length of the adaptive TMD	$Y_{2,1,20}$	$Y_{2,1,60}$	$Y_{2,1,80}$	$Y_{2,1}^{max}$
33-33-33 (L11)	2.1%	5.9%	6.3%	6.7%

TMD: tuned mass damper.
The test labels are those presented in Figure 9.

The different layouts tested and reported in Tables 2 and 4 evidence that the value of $Y_{2,1}^{max}$ can be changed significantly by changing the adaptive TMD configuration. Indeed, $Y_{2,1}^{max}$ changes from 2.6% to 5.0% in the considered cases.

As for the simulations for an adaptive TMD with three masses, the results are presented in Tables 6 and 7

Table 6. Maximum possible spans for the first three eigenfrequencies for different configurations of an adaptive TMD with three masses (with equal values, that is, 100 g) and four wires.

Percentage length of the four wires as function of the total length of the adaptive TMD	$Y_{2,1}^{max}$	$Y_{3,1}^{max}$	$Y_{3,2}^{max}$
25-25-25-25 (L12)	2.5%	4.8%	2.6%
10-40-40-10 (L14)	2.2%	1.3%	1.1%
40-10-10-40 (L15)	4.0%	4.8%	1.0%
10-20-30-40 (L16)	3.8%	3.2%	4.9%

TMD: tuned mass damper.
The test labels are those presented in Figure 9.

Table 7. Maximum possible spans for the first three eigenfrequencies of an adaptive TMD with three masses (with equal values, that is, 100 g) and four wires (H^{cur} = 7%).

Percentage length of the four wires as function of the total length of the adaptive TMD	$Y_{2,1}^{max}$	$Y_{3,1}^{max}$	$Y_{3,2}^{max}$
25-25-25-25 (L13)	3.4%	7.4%	3.8%

TMD: tuned mass damper.
The test labels are those presented in Figure 9.

(see also Figures 10(c) and (d)). Again, it is clear that the proposed adaptive TMD offers the possibility of tuning different eigenfrequencies with a certain amount of independency.

To summarise, a change in the initial geometry can be exploited in order to change the eigenfrequency values at environmental temperature: the increase/decrease of the mass values, the increase/decrease of the total length of the adaptive TMD and the decrease/increase of the axial load allow decreases/increases in the eigenfrequencies. Once these parameters are set, the envelope of the points describing the eigenfrequency values depends on the positions of the masses and on the mass ratio, which is able to widen the envelope. As for the adaptation capability, it still depends on the position of the masses, on the mass ratio, and on the number of the masses. Values of $Y_{2,1}^{max}$ over 4% can be achieved with $H^{cur} = 4.39\%$. However, the use of an SMA with a higher H^{cur} increases the values of $Y_{z,g}^{max}$ and thus improves the adaptation capability of the adaptive TMD.

It now has to be understood whether the spans reported in the previous tables are sufficient for practical applications. Indeed, it is important to understand not only which frequency shifts are experienced by each eigenfrequency of a real system but also the relative

Table 8. Data at T_{rif} = 20 °C for the beam considered in the example.

E_b (GPa)	L_b (m)	A_b (cm^2)	α_b (mm/m/ °C)	m_b (kg/m)	F_b (kN)
196	5	9 (square section)	0.0165	7.12	225

shift among the various resonance frequencies considered. Indeed, although the first aspect could barely constitute a real limit (it is rare to face a shift of more than 100%; for example, shifts due to thermal changes are usually around a few percentage points), the second point must be deepened. If the case of thermal changes is considered, the proposed layout is expected to work properly when equal percentage shifts are experienced by all the eigenfrequencies of the primary system. Nevertheless, when the relative shifts among the system eigenfrequencies are not known a priori, or the shifts of the different eigenfrequencies are not equal in percentage, the applicability of the device must be checked. To this purpose, the practical case of tensioned beams was studied. These elements are used in many engineering structures and are often flexible. Therefore, the damping of their vibrations is a common problem in many practical cases. Due to environmental changes during the year, the tensioned beams have to work in wide ranges of temperature: e.g. between −10 °C and 30 °C. The analytical expression of the kth eigenfrequency of a tensioned beam (for bending vibrations) is (Cheli and Diana, 2015)

$$\omega_k = k\frac{\pi}{L_b}\sqrt{\frac{F_b + E_b I_b\left(\frac{k\pi}{L_b}\right)^2}{m_b}} \tag{30}$$

where L_b is the beam length, F_b is the axial load in the beam, E_b is Young's modulus of the beam, I_b is the area moment of inertia of the beam cross section about the axis of interest and m_b is the mass per unit length of the beam. When the temperature changes, some properties of the beam change as well. Furthermore, also the axial load changes because of the thermal expansion/contraction. Since a tensioned beam with fixed position of the constraints is taken into account (in the linear field) in this example, the strain ε_b of the beam is constant, and the following relation holds

$$\begin{aligned}&\frac{F_b}{E_b A_b} + \alpha_b(T_b - T_{rif}) = \varepsilon_b \Rightarrow F_b \\ &= [\varepsilon_b - \alpha_b(T_b - T_{rif})]E_b A_b\end{aligned} \tag{31}$$

where A_b is the cross-sectional area of the beam, α_b is its thermal expansion coefficient, T_b is the beam temperature and T_{rif} is a reference temperature (chosen to be 20 °C here) at which the values of the other parameters are given (see, as an example, Table 8). Substituting equation (31) into equation (30), the following expression is achieved

$$\omega_k = k\frac{\pi}{L_b}\sqrt{\frac{\varepsilon_b E_b A_b - E_b A_b \alpha_b (T_b - T_{rif}) + E_b I_b\left(\frac{k\pi}{L_b}\right)^2}{m_b}} \tag{32}$$

If, as an example, the data of Table 8 are used and a temperature range between −10 °C and 30 °C is considered for T_b, the results of Table 9 are obtained. The value of s_1–s_2 was computed, where s_1 is the percentage shift of ω_1 and s_2 is the percentage shift of ω_2 compared to their values at 20 °C. If s_1–s_2 is null, an adaptive TMD with a null value of $Y_{2,1}^{max}$ is in theory enough to obtain tuning between the primary system and the adaptive TMD after an eigenfrequency change. Conversely, if s_1–s_2 is not null, the two eigenfrequencies change differently and $Y_{2,1}^{max}$ must be higher than s_1–s_2 to have the possibility of tuning both the adaptive TMD eigenfrequencies to those of the primary system after the shift. Table 9 shows values of $|s_1$–$s_2|$ always lower than 1.1%. Therefore, these results show that the adaptive TMD presented in this article would be able to adapt its eigenfrequencies properly, avoiding mistuning between the adaptive TMD and the primary system. Indeed, the changes in the first and the second eigenfrequency of the tensioned beam are much lower than 100%, so the adaptive TMD can follow their changes. Moreover, the values of $|s_1 - s_2|$ are always lower than 1.1%, while the Y values in Tables 2 to 7 are usually higher than 1.1%. This means that the proposed adaptive TMD is fully able to adapt its eigenfrequencies to those of the primary system and provide an optimal damping action.

Experiments

This section describes the experimental tests carried out to show the effectiveness of the presented multi-modal SMA-based adaptive TMD in adapting its dynamic characteristics. The next three subsections treat the experimental set-up, some issues to be considered when collecting measurements and their effects on result accuracy, and the results of the tests, respectively.

Set-up

The set-up used was based on SMA wires (Nitinol), manufactured by SAES Getters, whose characteristics were identified experimentally (see Table 1), and on

Table 9. Beam vertical eigenfrequencies (neglecting the change of α_b and E_b with temperature).

T (°C)	$\omega_1/(2\pi)$ (Hz)	Percentage shift of ω_1 compared to the value at T_{rif} = 20 °C (named s_1) (%)	$\omega_2/(2\pi)$ (Hz)	Percentage shift of ω_2 compared to the value at T_{rif} = 20 °C (named s_2) (%)	s_1–s_2 (%)
−10	21.14	17.56	43.31	16.53	1.03
0	20.14	12.01	41.36	11.28	0.73
10	19.09	6.17	39.32	5.79	0.38
20	17.98	0.00	37.17	0.00	0.00
30	16.80	−6.57	34.89	−6.14	−0.43

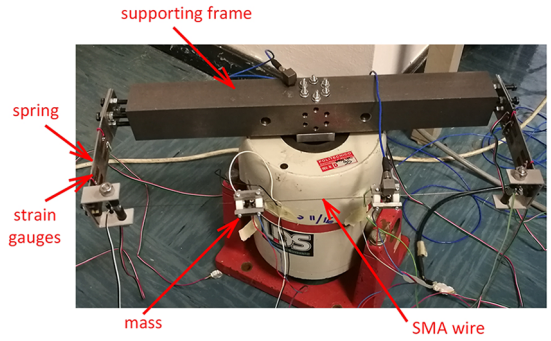

Figure 11. Experimental set-up with two masses and three SMA wires.

two masses of 18 g. The nominal diameter of the wires was 0.5 mm and the maximum admissible current (given by the manufacturer) was 5.0 A. The elastic elements were steel cantilever beams, provided with calibrated strain gauge Wheatstone bridges (Doebelin, 2003) with temperature compensation, aimed at measuring the axial load on the wires. The value of K was set in order to have a range of σ_w between about 80 MPa (with all the wires at environmental temperature, 20 °C) and 205 MPa (with all the wires in AU condition thanks to heating). The global length of the adaptive TMD was 35 cm. It was verified that the adaptive TMD configuration was approximately rectilinear in the static equilibrium position (static deflections significantly lower than 1 mm).

The set-up was directly mounted on a shaker, using a supporting frame, to provide the random disturbance in the vertical direction (see Figure 11). The disturbance was provided in the frequency range of the first two vertical eigenfrequencies of the adaptive TMD (estimated by using its analytical model), and its root mean square (RMS) value was between 2 and 8 m/s^2, depending on the test considered. The frequency band of the provided noise was usually 10 or 15 Hz wide.

The electric resistance values of the wires were measured at environmental temperature and resulted as being 0.7 Ω for each of the wires. One independent external power supplier was used to feed each wire. The constant current supplied to each wire was measured every time and the maximum value used in the experiments was 2.1 A.

In each test, the axial load on the wires was measured and changed by heating one or more of them. The first two vertical eigenfrequencies of the adaptive TMD were experimentally identified by means of a modal analysis (Peeters et al., 2004) each time. The starting data for the modal identification were the frequency response functions (FRF) measured between an accelerometer measuring the vertical vibration of the supporting frame (see Figure 11) and the vibration of the two masses of the adaptive TMD. A contactless laser Doppler velocimeter was used for one of the masses, while for the other an accelerometer was placed on the mass. The weight of the accelerometer was equal to 5 g, and this additional mass was taken into account when carrying out the simulations of the adaptive TMD dynamics. Therefore, one mass of the adaptive TMD was set at 18 g and the other at 23 g in the simulations. The two masses had a cylindrical shape. The FRFs were estimated using the H_1 estimator (Brandt, 2011).

At environmental temperature, the first two eigenfrequencies resulted to be about 12.9 and 22.2 Hz, which are close to the theoretical expectations of 13.8 and 24.4 Hz. The first mode had the two masses moving in phase, while the second was characterised by an out-of-phase vibration, as expected from theory and simulations.

Figure 12(a) shows the FRF for one of the two masses with all the wires at environmental temperature. There is a small peak in the FRF after the second eigenfrequency. This peak is due to a resonance of the adaptive TMD in the horizontal direction. Indeed, it was very difficult to measure the vibrations of the two masses of the adaptive TMD exactly along the principal axes. However, this low-amplitude peak did not cause any problem in the identification of the two eigenfrequencies considered here.

Result accuracy

Under a theoretical point of view, the tests on the set-up of Figure 11 would require a given current value for each wire to be fixed and the corresponding eigenfrequencies of the adaptive TMD to be estimated. After this, a comparison with the numerical results, imposing the same current values in the model, would have

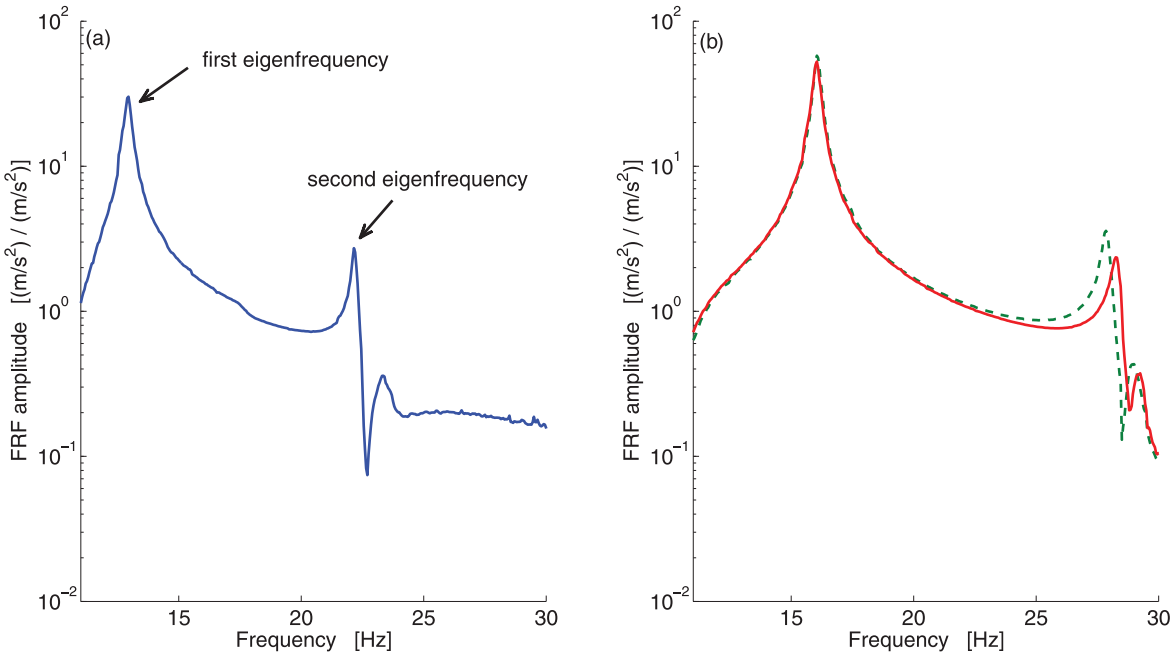

Figure 12. FRF amplitude between the accelerometer on the supporting frame and the accelerometer on one of the two masses: (a) adaptive TMD with all the wires at environmental temperature and (b) adaptive TMD in the conditions of test 2 of Table 10 (green dashed line) and in the conditions of test 3 of Table 10 (red solid line).

allowed model validation. However, some problems arose during the tests, related to the fact that the resistance value of the SMA wires can undergo slight changes when heated. If the current flowing into the wires is measured and the thermal model discussed previously (see equation (3)) is used to estimate the temperature of the wires, these small resistance changes (which cannot be measured and are thus unknown) result in bias effects on the temperature estimations. Moreover, it is also difficult to accurately estimate the value of the convection coefficient h for the vibrating strings, which becomes another source of bias effects. A nominal value of 130 W/m^2/ °C was used in the simulations for h. The amplitude of the vibration, however, causes a change in h; therefore, the nominal value used for h is affected by an unknown bias. These bias effects, even if small, have a large effect on the resulting eigenfrequencies. Indeed, when the SMA wire is in transformation between DM and AU or vice versa, a small change in temperature can significantly change the resulting eigenfrequency values (i.e. changes in the order of a few Hertz).

To overcome these problems, one possibility could be to model the behaviour of the resistance values as a function of the flowing current and the temperature of the wires (and the value of h should be investigated as function of the vibration amplitude as well). However, this was considered beyond the scope of this work and would not have added anything to it. Another possibility would be to validate the adaptive TMD behaviour in terms of the shifts achievable on both eigenfrequencies without considering the actual current value needed to obtain it. This means, in practice, comparing the theoretical eigenfrequency plot with the experimental one. Thanks to its simplicity, this approach was followed to carry out the tests. As a first step, the numerical plot was thus derived for the considered system, and many points describing the values of the second eigenfrequency of the adaptive TMD as a function of the first one were derived. The model can be considered validated if the experimental points describe the same area described by the numerical results. For this reason, many experimental tests were carried out changing the current flowing into the wires, which made it possible to place many experimental results on the same plot of the numerical results, and therefore make a direct comparison.

Experimental results and model validation

The experimental tests were performed by changing the currents flowing into the three wires. A total of 42 tests were carried out. The main data related to some of these tests (those discussed in detail in this section) are presented in Table 10. Here, F^{meas} is the measured axial load acting on the wires. This load is the static load applied (and measured) before switching on the shaker. When the vibration starts, the axial load obviously changes continuously, maintaining the value measured prior to excitation of the adaptive TMD as the mean value. The peaks of the axial load signals were found to

Table 10. Measured/identified data for the tests carried out.

Test number	i_w^1 (A)	d_w^1	i_w^2 (A)	d_w^2	i_w^3 (A)	d_w^3	F^{meas} (N)	$\omega_1/(2\pi)$ (Hz)	$\omega_2/(2\pi)$ (Hz)
1	0.000	+	0.000	+	0.000	+	15.70	12.95	22.15
2	0.000	+	0.000	+	2.030	+	24.15	16.05	27.85
3	0.000	+	1.010	+	0.850	−	24.17	16.05	28.25
4	0.000	+	2.040	+	2.050	+	33.19	18.75	32.50
5	0.840	−	0.912	−	2.020	+	33.15	18.75	33.10
6	2.024	+	1.133	+	2.100	+	42.70	21.60	38.25

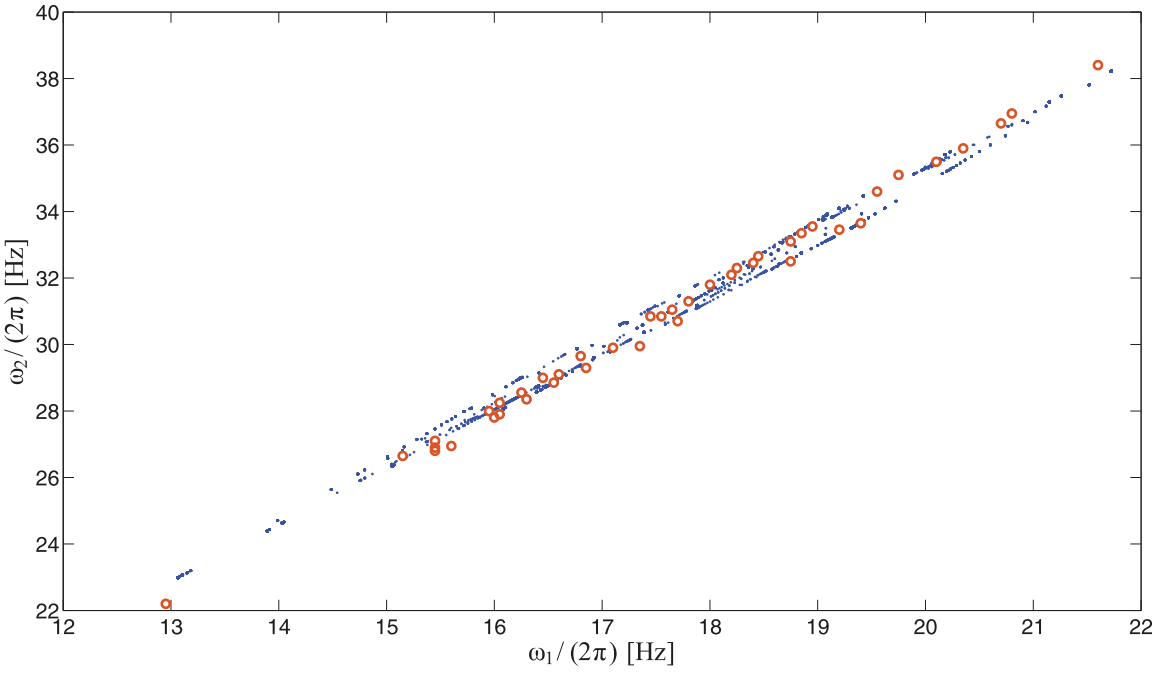

Figure 13. Relationship between the first and the second eigenfrequencies; the experimental results are the red circles, while the numerical results are the blue dots.

differ from the mean value by a quantity significantly lower than 1 N and thus negligible.

Furthermore, in Table 10, i_w^r is the current flowing in the rth wire, d_w^r indicates the sign of the change of the current flowing in the rth wire with respect to a reference configuration with a + or a −. When the sign is negative, it means that the wire was previously heated to above the AU temperature and then cooled until the considered current was reached. Conversely, a positive sign means that the current was increased directly from the DM condition. It is remarked that the directions of change (i.e. increase/decrease) of the current flowing in each wire, with respect to the previous test configuration, are important data for fully understanding the layout of the tests because of the hysteretic behaviour of SMA materials on the stress–temperature plane (Lagoudas, 2008). Among the experiments conducted, there was also a test with no current flowing in the wires (i.e. a test at environmental temperature with all the wires in DM; test 1 in Table 10) and a test where all the wires were heated to AU, which caused the maximum possible values of the first and second eigenfrequencies of the adaptive TMD (test 6 in Table 10).

Every time the current was changed in at least one wire, the steady-state condition of the system was waited for before collecting the vibration data used to estimate the FRFs of the adaptive TMD. The achievement of the steady-state condition was monitored by analysing the signals coming from the calibrated Wheatstone bridges on the elastic beams (see Figure 11).

The resulting relationship between the first and the second eigenfrequencies of the adaptive TMD is plotted in Figure 13 considering all the experiments carried out. The maximum experimental percentage change of the first eigenfrequency with the maximum and minimum values of σ_w chosen for this set-up (see previously) was found to be 66.8%, while the numerical

expectation was 66.2%. Figure 13 evidences that the experimental points are well superimposed on the numerical ones. Furthermore, there are many situations where a different second eigenfrequency value corresponds to the same value of the first eigenfrequency or vice versa. As an example, the value of $Y_{2,1,45}$ (in correspondence to a value of the first eigenfrequency equal to about 18.75 Hz, see tests 4 and 5 in Table 10) is about 2.72%. At the same first eigenfrequency value, the result expected from the simulations is 3.02%, which is close to the result obtained experimentally. Moreover, the envelope of the experimental points is close to that of the numerical points.

As an example, Figure 12(b) shows two FRFs (those of tests 2 and 3 of Table 10), where the first eigenfrequency is at the same value, but the value of the second eigenfrequency shows an evident difference between the two curves.

Conclusion

This article has dealt with an innovative adaptive TMD based on SMA wires. This device is able to change two (or more) of its eigenfrequencies at the same time with a certain degree of independency. This is made possible by designing the adaptive TMD with two (or more) masses linked by SMA wires and heating each wire independently from the others, generating a change of the axial load in the wires and a change of the TMD geometry. When a single wire is heated, the other wires can undergo a phase transformation, thanks to the pseudoelastic effect of SMA materials, even if their temperature is not changed by either heating or cooling. This allows an increase in the possible dynamic configurations of a single device.

A model of the proposed device was developed, composed of three different models: a thermal model, a model of the material and a dynamic model.

Numerical simulations were carried out at first in order to find how to change the initial values of the eigenfrequencies and then to test the adaptation capability of the new device. As for the first point, it was found that a change in the initial geometry could be exploited to change the eigenfrequency values at environmental temperature: the increase/decrease of the mass values, the increase/decrease of the total length of the adaptive TMD and the decrease/increase of the axial load make it possible to decrease/increase the eigenfrequencies. Once these parameters are set, the envelope of the points describing the value of each eigenfrequency as a function of the others depends on the positions of the masses and on the mass ratio, which widens the envelope. As for the adaptation capability, it still depends on the position of the masses, on the mass ratio and on the number of the masses. The adaptation capability of the adaptive TMD can be increased also using SMA wires with high H^{cur} values; the higher H^{cur} is, the higher the values of $Y_{z,g}^{\max}$ will be.

An experimental campaign was carried out on a set-up made from two masses and three wires. The model was validated, showing that the designed adaptive TMD is actually able to change the first two eigenfrequencies in a wide frequency range and set its second eigenfrequency at different values, while the first one remains at the same value.

This kind of adaptive TMD can be easily coupled to devices able to adapt damping as well, allowing for a fully adaptive device.

Declaration of conflicting interests

The author(s) declared no potential conflicts of interest with respect to the research, authorship and/or publication of this article.

Funding

The author(s) received no financial support for the research, authorship and/or publication of this article.

Marta Berardengo https://orcid.org/0000-0002-8625-0822
Stefano Manzoni https://orcid.org/0000-0002-9240-5472

References

Acar MA and Yilmaz C (2013) Design of an adaptive–passive dynamic vibration absorber composed of a string–mass system equipped with negative stiffness tension adjusting mechanism. *Journal of Sound and Vibration* 332: 231–245.

Aguiar RA, Savi MA and Pacheco PM (2012) Experimental investigation of vibration reduction using shape memory alloys. *Journal of Intelligent Materials Systems and Structures* 24: 247–261.

Berardengo M, Cigada A, Guanziroli F, et al. (2014) An adaptive tuned mass damper based on shape memory alloys with an extended range of frequency. In: *Proceedings of EESMS 2014–2014 IEEE workshop on environmental, energy and structural monitoring systems*, Naples, 17–18 September 2014, pp. 90–95. New York: IEEE.

Berardengo M, Cigada A, Guanziroli F, et al. (2015a) Modelling and control of an adaptive tuned mass damper based on shape memory alloys and eddy currents. *Journal of Sound and Vibration* 349: 18–38.

Berardengo M, Manzoni S and Conti AM (2017a) Multimode passive piezoelectric shunt damping by means of matrix inequalities. *Journal of Sound and Vibration* 405: 287–305.

Berardengo M, Manzoni S and Vanali M (2016) The behaviour of mistuned piezoelectric shunt systems and its estimation. *Shock and Vibration* 2016: 9739217.

Berardengo M, Manzoni S, Thomas O, et al. (2015b) A new electrical circuit with negative capacitances to enhance resistive shunt damping. In: *Proceedings of the ASME 2015 conference on smart materials, adaptive structures and intelligent systems*, Colorado Springs, CO, 21–23 September 2015, p. V001T03A006. New York: ASME.

Berardengo M, Thomas O, Giraud-Audine C, et al. (2017b) Improved shunt damping with two negative capacitances: an efficient alternative to resonant shunt. *Journal of Intelligent Materials Systems and Structures* 28: 2222–2238.

Brandt A (2011) *Noise and vibration analysis: Signal analysis and experimental procedures*. Chichester: Wiley.

Casciati S, Isalgue A, Torra V, et al. (2014) SMA passive elements for damping in the stayed cables of bridges. In: Belyaev A, Irschik H and Krommer M (eds) *Mechanics and Model-Based Control of Advanced Engineering Systems*. New York: Springer, pp. 75–83.

Caterino N, Spizzuoco M and Occhiuzzi A (2011) Understanding and modelling the physical behaviour of magnetorheological dampers for seismic structural control. *Smart Materials and Structures* 20: 065013.

Cheli F and Diana G (2015) *Advanced Dynamics of Mechanical Systems*. New York: Springer.

Dai H, Huang Z and Wang W (2014) A new permanent magnetic friction damper device for passive energy dissipation. *Smart Materials and Structures* 23: 105016.

Dieng L, Helbert G, Chirani SA, et al. (2013) Use of shape memory alloys damper device to mitigate vibration amplitudes of bridge cables. *Engineering Structures* 56: 1547–1556.

Doebelin E (2003) *Measurement Systems: Application and Design*. New York: McGraw-Hill.

dos Santos FA and Nunes J (2018) Toward an adaptive vibration absorber using shape-memory alloys, for civil engineering applications. *Journal of Intelligent Materials Systems and Structures* 29: 729–740.

Gómez BJ, Repetto CE, Stia CR, et al. (2007) Oscillations of a string with concentrated masses. *European Journal of Physics* 28: 961–975.

Heuss O, Salloum R, Mayer D, et al. (2016) Tuning of a vibration absorber with shunted piezoelectric transducers. *Archive of Applied Mechanics* 86: 1715–1732.

Høgsberg J and Krenk S (2015) Balanced calibration of resonant piezoelectric RL shunts with quasi-static background flexibility correction. *Journal of Sound and Vibration* 341: 16–30.

Lagoudas DC (2008) *Shape Memory Alloys: Modeling and Engineering Applications*. New York: Springer.

Majewska K, Żak A and Ostachowicz W (2007) Magnetic shape memory alloys for forced vibration control of beam-like structures. *Smart Materials and Structures* 16: 2388–2397.

Mani Y and Senthilkumar M (2013) Shape memory alloy based adaptive-passive dynamic vibration absorber for vibration control in piping applications. *Journal of Vibration and Control* 21: 1838–1847.

Mavroidis C (2002) Development of advanced actuators using shape memory alloys and electrorheological fluids. *Research in Nondestructive Evaluation* 14: 1–32.

Meirovitch L (2001) *Fundamentals of Vibrations*. New York: McGraw-Hill.

Ozbulut OE, Mir C, Moroni MO, et al. (2007) A fuzzy model of superelastic shape memory alloys for vibration control in civil engineering applications. *Smart Materials and Structures* 16: 818–829.

Peeters B, Lowet G, Van der Auweraer H, et al. (2004) A new procedure for modal parameter estimation. *Journal of Sound and Vibration* 38: 24–28.

Piccirillo V, Balthazar JM, Tusset AM, et al. (2016) Application of a shape memory absorber in vibration suppression. *Applied Mechanics and Materials* 849: 27–35.

Rainieri C and Fabbrocino G (2015) Development and validation of an automated operational modal analysis algorithm for vibration-based monitoring and tensile load estimation. *Mechanical Systems & Signal Processing* 60: 512–534.

Rustighi E, Brennan MJ and Mace BR (2005a) A shape memory alloy adaptive tuned vibration absorber: design and implementation. *Smart Materials and Structures* 14: 19–28.

Rustighi E, Brennan MJ and Mace BR (2005b) Real-time control of a shape memory alloy adaptive tuned vibration absorber. *Smart Materials and Structures* 14: 1184–1195.

Saggin B, Scaccabarozzi D, Tarbini M, et al. (2017) Design of a smart bidirectional actuator for space operation. *Smart Materials and Structures* 26: 035041.

Savi MA, De Paula AS and Lagoudas DC (2010) Numerical investigation of an adaptive vibration absorber using shape memory alloys. *Journal of Intelligent Materials Systems and Structures* 22: 67–80.

Senthilkumar P and Umapathy M (2013) Use of load generated by a shape memory alloy for its position control with a neural network estimator. *Journal of Vibration and Control* 20: 1707–1717.

Tiseo B, Concilio A, Ameduri S, et al. (2010) A shape memory alloys based tunable dynamic vibration absorber for vibration tonal control. *Journal of Theoretical and Applied Mechanics* 48: 135–153.

Torra V, Carreras G, Casciati S, et al. (2014) On the NiTi wires in dampers for stayed cables. *Smart Structures and Systems* 13: 353–374.

Weber F (2013) Dynamic characteristics of controlled MR-STMDs of Wolgograd Bridge. *Smart Materials and Structures* 22: 095008.

Weber F and Maślanka M (2012) Frequency and damping adaptation of a TMD with controlled MR damper. *Smart Materials and Structures* 21: 055011.

Williams KA, Chiu GT-C and Bernhard RJ (2002) Adaptive-passive absorbers using shape-memory alloys. *Journal of Sound and Vibration* 249: 835–848.

Williams KA, Chiu GT-C and Bernhard RJ (2005) Nonlinear control of a shape memory alloy adaptive tuned vibration absorber. *Journal of Sound and Vibration* 288: 1131–1155.

Zuo X and Li A (2011) Numerical and experimental investigation on cable vibration mitigation using shape memory alloy damper. *Structural Control & Health Monitoring* 18: 20–39.